applied sciences

MDPI

Article

Assessing the Wind Energy Potential: A Case Study in Fort Hare, South Africa, Using Six Statistical Distribution Models

Ngwarai Shambira *, Patrick Mukumba and Golden Makaka

Physics Department, Faculty of Science & Agriculture, University of Fort Hare, Alice 5700, South Africa; pmukumba@ufh.ac.za (P.M.); medzai9@gmail.com (G.M.)
* Correspondence: nshambira@ufh.ac.za

Abstract: Wind energy is a clean, inexhaustible resource with significant potential to reduce coal dependence, lower carbon emissions, and provide sustainable energy in the off-grid areas of South Africa's Eastern Cape. However, due to wind variability, site-specific assessments are crucial for accurate resource estimation and investment risk mitigation. This study evaluates the wind energy potential at Fort Hare using six statistical distribution models: Weibull (WEI), Rayleigh (RAY), gamma (GAM), generalized extreme value (GEV), inverse Gaussian (IGA), and Gumbel (GUM). The analysis is based on three years (2021–2023) of hourly wind speed data at 10 m above ground level from the Fort Beaufort weather station. Parameters were estimated using the maximum likelihood method (MLM), and model performance was ranked using the total error (TE) metric. The results indicate an average wind speed of 2.60 m/s with a standard deviation of 1.85 m/s. The GEV distribution was the best fit (TE = 0.020), while the widely used Weibull distribution ranked third (TE = 0.5421), highlighting its limitations in capturing wind variability and extremes. This study underscores the importance of testing multiple models for accurate wind characterization and suggests improving the performance of the Weibull model through advanced parameter optimization, such as artificial intelligence. The wind power density was 31.52 W/m^2, classifying the site as poor for large-scale electricity generation. The prevailing wind direction was southeast. Recommendations include deploying small-scale turbines and exploring augmentative systems to optimize wind energy utilization in the region.

Keywords: Weibull distribution; wind speed; wind direction; wind energy; wind power density

Academic Editors: Piotr Pawłowski, Ryszard Szwaba, Małgorzata A. Śmiałek and Janusz Telega

Received: 22 January 2025
Revised: 26 February 2025
Accepted: 3 March 2025
Published: 5 March 2025

Citation: Shambira, N.; Mukumba, P.; Makaka, G. Assessing the Wind Energy Potential: A Case Study in Fort Hare, South Africa, Using Six Statistical Distribution Models. *Appl. Sci.* **2025**, *15*, 2778. https://doi.org/10.3390/app15052778

1. Introduction

South Africa faces significant energy challenges, with approximately 3.5 million rural households lacking access to electricity and relying on traditional biomass due to financial constraints or the absence of grid connections [1–4]. Limpopo Province has the highest electricity access rate at 98.55%, while the Eastern Cape lags at 82% [5]. These issues are compounded by South Africa's national power utility, Eskom, which faces a USD 24 billion debt, aging infrastructure, and corruption. These challenges hinder electricity supply and result in frequent load shedding as energy demand continues to rise [6]. Wind energy presents a viable solution, with the South African wind energy association estimating it could meet 62% of the country's energy needs [7]. Additionally, the Renewable Energy Independent Power Producer Procurement Programme (REIPPPP) reported a 42% reduction in wind energy production costs, bringing it down to 74 cents per kWh [8].

Global wind energy capacity grew from 743 GW in 2020 to 837 GW in 2021, with China and the United States leading at 338 GW and 134 GW, respectively. According to the Global Wind Energy Council, this expansion reduced carbon dioxide emissions by over 637 million tonnes, contributing significantly to climate change mitigation [9]. These reductions are crucial in addressing extreme weather events, such as the heatwaves experienced in Cape Town and cyclones that have impacted Mozambique and Zimbabwe [10].

1.1. An Overview of Wind Energy Utilization in South Africa

Wind energy, one of the oldest energy sources, dates back to ancient times when it was primarily used for grinding grain, pumping water for drinking, and irrigation [1]. In the 1990s, around 30,000 windmills were installed in South Africa to provide drinking water and support agricultural activities [11,12]. Despite having significant wind energy potential, particularly in the Eastern Cape, Western Cape, Northern Cape, and KwaZulu-Natal, South Africa has historically prioritized cheaper coal over wind energy for electricity generation [12,13]. Out of 410,000 km^2 of land exposed to wind speeds over 6.5 m/s, only 1174 km^2 is designated for wind farms [13]. Coastal regions have an annual mean wind speed of 6 m/s at a height of 10 m above ground level, with an estimated high wind potential of 60 TWh annually [14]. However, wind potential varies with time and location, necessitating site-specific wind resource assessments to reduce investment risks by selecting suitable wind turbines [1,15]. Statistical analysis of wind characteristics is also crucial for optimizing wind energy utilization (McKenna et al., 2021). As a leading country in wind energy technology in Africa, South Africa attracted ZAR 209.7 billion in investments for wind energy projects in 2020. The wind energy sector has created 2723 jobs, commercialized 22 independent power producers, and reduced carbon dioxide emissions by 6.4 million tonnes [16]. Since the first large-scale wind farm was installed in 2014, South Africa now has 33 wind farms, with 22 fully operational and the rest under construction [17]. Figure 1 depicts some of the wind farms and their capacity in South Africa.

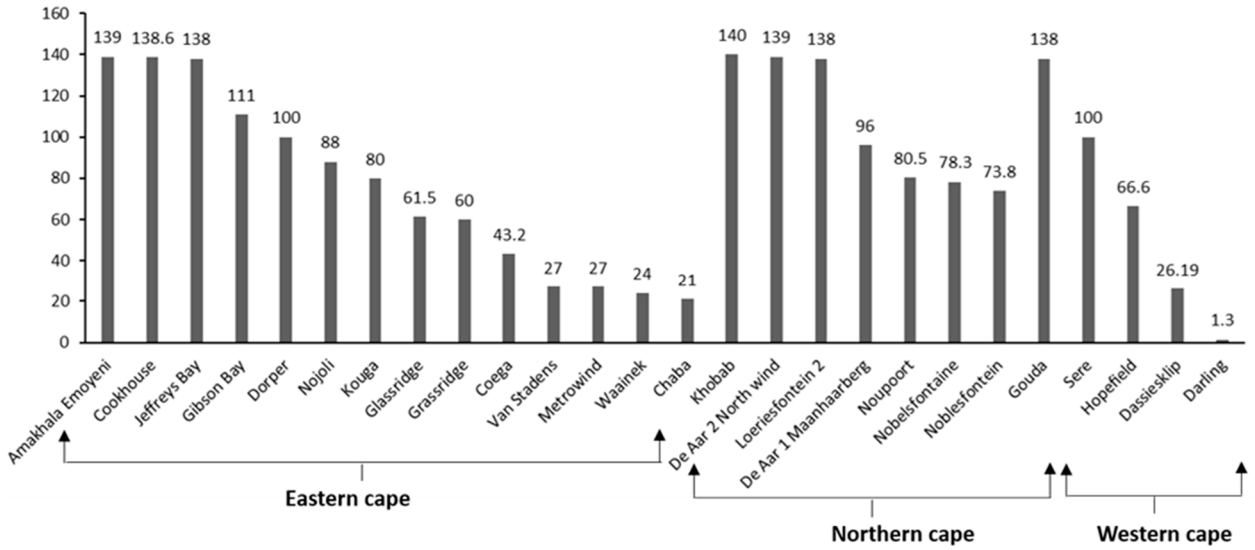

Figure 1. Wind farms in South Africa and their capacity (MW) [11].

As depicted in Figure 1, Jeffreys Bay in the Eastern Cape Province is one of South Africa's largest wind farms, covering 3700 hectares. However, Amakhala Emoyeni and Cookhouse, also in the Eastern Cape, have higher capacities at 139 MW and 138.6 MW, respectively. Jeffreys Bay's proximity to the national grid, flat topography, and minimal environmental impacts make it an ideal wind resource location. In the Northern Cape, the Khobab, De Aar 2 North, and Loeriesfontein 2 wind farms have capacities of 140 MW,

139 MW, and 138 MW, respectively. The Noupoort wind farm, covering 7500 hectares with an 80 MW capacity, benefits from excellent wind conditions and proximity to the national grid and roads, facilitating easy transport and construction of wind turbines [16]. The Northern Cape leads in wind farm investment costs, with De Aar 2 North costing ZAR 5 billion and both Loeriesfontein 2 and Khobab wind farms costing ZAR 3.5 billion each. In the Eastern Cape, Amakhala Emoyeni's investment cost is ZAR 3.94 billion, while Jeffreys Bay and Cookhouse are valued at ZAR 2.9 billion and ZAR 2.4 billion, respectively. In the Western Cape, the Gouda wind farm's investment cost is ZAR 2.7 billion. These investments highlight South Africa's commitment to integrating wind energy into its energy mix, demonstrating its leadership in wind energy technology in Africa. Between 2011 and 2015, wind energy prices decreased by 20% to ZAR 0.62 per kWh, making them ZAR 0.41 cheaper than coal prices [13,17]. By 2030, it is anticipated that 11,800 MW to 12,500 MW of South Africa's power will come from wind energy [18].

1.2. Related Literature on Wind Potential Assessment

Wind data are often treated as a continuous random variable, requiring continuous probability distributions for modeling predictable wind patterns [19]. Among these, the two-parameter Weibull (WEI) distribution is widely used, though its performance varies depending on location and wind regimes [20,21]. Studies often explore alternative distributions to determine the most suitable model for specific regions. For instance, ref. [22] investigated the wind potential across nine Nigerian locations, identifying the Rayleigh (RAY) distribution as the best fit for six sites, while the log-normal (LGN) distribution was superior for Maiduguri, Abuja, and Akure. Similarly, ref. [23] analyzed wind speed characteristics using both commonly used distributions (Generalized Rayleigh (GR), GAM, GUM, Exponentiated Weibull (EW)) and more recent ones (Exponentiated Half-Logistic (EHL), Exponentiated Half-Normal (EHN), Skew Logistic (SL), and Generalized Extreme Value (GEV)) at seven meteorological stations in northern Iran. The study found that the EHN distribution provided the best overall fit.

A study conducted by [24] assessed 44 wind speed distribution models in Lebanon, finding the Wakeby (WAK) and Beta distributions to be generally the best. The WAK distribution provided the best fit for Younine, Birket Aarous, Mqaybleh, and Hekr El Dahri, while the Beta distribution was the best fit for Khiam, Iskandarounah, Khartoum, and Qaraoun. Gumbel Min and generalized logistic were best for Ain ed Dabaa and Ras Ouadi Ed Darje, respectively. Likewise, ref. [25] assessed various wind speed distribution models in Malaysia using goodness-of-fit criteria like the coefficient of determination (COD), Kolmogorov–Smirnov statistic (KSS), Akaike's information criterion (AIC), and skewness/kurtosis deviation (SKDEV). Eight distributions, including LGN, WEI, RAY, exponential, Burr, GAM, inverse Gaussian (IGA), and inverse gamma, were tested on data from Kuantan and Balok Baru. The GAM distribution was found to be the best fit for wind speed data at both locations.

Ref. [26] evaluated the wind power potential at eight sites in northern Cyprus using wind data collected from Lefkoşa. Their analysis revealed that the GEV distribution provided the best fit for Lefkoşa, Ercan, Girne, Güzelyurt, and Dipkarpaz. In contrast, the log-logistic (LL), WEI, and GAM distributions were more accurate for Gazimağusa, YeniBoğaziçi, and Salamis, respectively. The RAY distribution, however, performed poorly across all sites. The study reported wind power densities ranging from 38.76 to 134.29 W/m^2, suggesting limited potential for large-scale energy production. Nevertheless, the 5 kW Aeolos-V2 wind turbine was identified as suitable for meeting household energy needs in the region. Also, ref. [27] conducted wind potential assessment in the Marmara Region, Turkey, using ten distributions. The GAM, Burr, and WEI distributions were found to be

superior, with metaheuristic methods enhancing parameter estimation accuracy. Ref. [28] evaluated onshore wind potential in seven southern Iranian coastal cities to reduce fossil fuel reliance. They analyzed six probability distributions, finding the WEI suitable for one station, GEV for three, and GAM for the rest. The study recommended the GAM distribution for its simplicity and effectiveness in assessing the region's wind energy potential. These studies from different countries confirm that the performance of wind speed distributions is site-specific.

Furthermore, the research presented in [19] reviewed fourteen probability distributions for wind speed data at seventeen Indian locations. The study found that the WEI distribution often struggled with heterogeneous data. The truncated normal–gamma distribution fit best at four locations, while the GAM distribution was most suitable at six locations among the two-parameter distributions. In contrast, the study by [29] assessed wind speed characterization at twelve Nigerian stations, comparing five distribution methods. Using the KSS, root mean square error (RMS), and chi-square (CHI) tests, they found that the Mixture Weibull method performed best overall, closely followed by LGN. The WEI and GAM distributions were less accurate, emphasizing the need to fit multiple distributions to find the most appropriate one, as the accuracy of a distribution in describing wind speed is site-specific.

In a study conducted by [30], along Turkey's Aegean coast, various distributions, including RAY, inverse Weibull (IW), Burr type III, extreme value (EV), GAM, inverse gamma (IG), Marshall–Olkin extended Lindley (MOEL), GEV, and EW, were analyzed for wind speed modeling. The EW distribution provided the best overall fit, followed by the GEV distribution. The WEI, EV, GAM, and MOEL distributions performed well in cases where skewness was less than one and kurtosis was below four. In contrast, the Burr type III, IW, and IG distributions were more effective for data with higher skewness and kurtosis values. RAY had the worst performance. Also, ref. [31] analyzed ten years of wind speed data from four stations in Johor, Malaysia, using the GAM, GEV, LGN, RAY, and WEI distributions. The GEV distribution provided the best fit for the Senai, Mersing, and Batu Pahat stations, while the GAM distribution was most suitable for Kluang.

In another study, ref. [32] assessed wind speed at ten sites in Tamil Nadu, India, using 39 years of historical data. They utilized nine distribution models, including exponential, GAM, GEV, IG, Kumaraswamy, LL, LGN, Nakagami, and WEI, to evaluate the wind characteristics. The study found that the GEV distribution was the most suitable for most stations, with Kumaraswamy also performing well, particularly for negatively skewed data. This highlighted the need to select different distributions based on varying topographical conditions. Similarly, ref. [33] evaluated wind speed at the Mersing station in Malaysia, comparing the GAM, GEV, LGN, RAY, and WEI distributions using the maximum likelihood method (MLM). Consistent with the findings of [32], the GEV distribution emerged as the best fit in this study, underscoring GEV's robustness in diverse geographical contexts.

In South Africa, ref. [34] assessed the wind energy potential in Mthatha, in Eastern Cape Province, using two-parameter and three-parameter Weibull distribution models. Their study utilized wind data collected at a 10 m height above ground level from 2018 to 2023. The analysis revealed low average wind speeds of 3.30 m/s and a wind power density of approximately 48.48 W/m^2. These findings indicate that the area may not be ideal for large-scale wind energy projects but is suitable for standalone applications. The prevailing wind directions were predominantly from the south and east–southeast. Similarly, ref. [10] evaluated the wind potential of Fort Beaufort, South Africa, using the two-parameter Weibull distribution. They applied eight numerical methods to determine the Weibull scale and shape parameters based on five-and-a-half years of hourly wind data. The study concluded that Fort Beaufort is suitable for small-scale wind energy projects

with prevailing southeast winds. The authors also recommended the use of augmented wind turbines incorporating concentrators and diffusers to improve efficiency in areas with low wind speeds.

The WEI distribution has been shown to be highly effective in several studies. For example, ref. [20] investigated the wind speed distribution in Agadir, Morocco, comparing the WEI, RAY, GAM, and LGN distributions. Their results, validated by goodness-of-fit tests, identified the WEI distribution as the most accurate model for estimating the annual wind power density. Consequently, they recommended the WEI distribution for wind energy assessments in the region. Similarly, ref. [35] analyzed wind speed data from Tarnab, Peshawar (2004–2023) using the WEI and RAY distributions. Their findings revealed that the WEI distribution closely matched the observed data, further affirming its superiority for wind energy analysis.

In Jordan [36], the wind energy potential across nine locations was assessed using WEI, RAY, and GAM distributions. Among the sites, King Hussein Airport exhibited the highest wind power density, with the WEI distribution again providing the best fit. Ref. [37] evaluated the wind energy potential in Omu Aran, Nigeria, over five years using the WEI and RAY distributions. Their analysis reported a mean yearly wind speed of 3.964 m/s, categorizing the location in wind power class 1. The WEI distribution demonstrated strong performance, making it suitable for preliminary wind power plant design in Kwara State. This study further highlighted the reliability of the WEI distribution for wind energy assessments.

Studies in Pakistan by [38,39] demonstrated the reliability of the WEI distribution in wind energy assessments. Ref. [38] assessed the wind energy potential in Jhimpir, Sindh, Pakistan, using eight probability distribution functions: WEI, RAY, GUM, LGN, Logistic (LOG), GAM, generalized Lindley (GL), and Cauchy distributions (CD). Based on 3 years and 6 months of wind speed data, their analysis identified the WEI and RAY distributions as the best-fitting models, with the WEI distribution showing slightly better performance. Wind power density estimates ranged from 84.67 to 698.65 W/m^2, indicating that the site is suitable for wind power production. The predominant wind directions were from the east and southeast. Similarly, ref. [39] assessed the wind power potential in Pakistan's Sindh, Balochistan, and Khyber Pakhtunkhwa Provinces, utilizing the WEI distribution. On the other hand, ref. [40] assessed the wind energy potential in southwestern Aceh coastal areas, Indonesia, using WEI and MLM. The wind power densities obtained ranged from 4590 to 26,040 W/m^2, classifying the site as low-class for wind power generation.

Most studies assessing the wind potential in the Eastern Cape Region of South Africa have predominantly relied on the two-parameter Weibull distribution. There has been limited exploration of other distributions. When alternatives have been considered, they have typically focused only on fitting without leveraging third-moment statistical properties to evaluate wind power densities or obtaining additional statistical measures such as mean, variance, skewness, and kurtosis from the determined distribution parameters. This study seeks to address this gap by applying multiple distributions, such as the Weibull (WEI), Rayleigh (RAY), gamma (GAM), generalized extreme value (GEV), inverse Gaussian (IGA), and Gumbel (GUM) methods, to determine the most suitable distribution for the location and to assess the statistical properties and wind power density of the area.

Section 2 details the materials and methods used in this research, including a description of the site, its location, the source of the wind data, and an overview of the distribution models and numerical methods for parameter estimation. It also covers the test statistics used for the goodness-of-fit analysis. Section 3 presents and discusses the main results of the study, while Section 4 concludes with a summary of the findings and recommendations.

2. Materials and Methods

2.1. Site Description and Wind Speed Data

This study utilized three years of hourly average wind speed data from January 2021 to December 2023, collected from the Fort Beaufort weather station located at a latitude of −32.7880, a longitude of 26.6290, and an altitude of 455 m in the Eastern Cape Province, South Africa. The wind speed data, recorded at an anemometer height of 10 m above ground level, were sourced from the South African Weather Service. Figure 2 presents a geographical map of the study location.

Figure 2. Location of study area.

2.2. Statistical Probability Distribution Models

Wind speed profile characterization is crucial in assessing wind availability at a particular location [21]. Six different distributions are introduced to characterize the distribution of wind speeds. A brief explanation of these distributions is provided below. The other statistical properties (SPs) of each distribution are reported in Tables 1–6, namely, mean wind speed ($\overline{v}_{dist}$), variance ($\sigma^2{}_{dist}$), third moment (μ_3), skewness (S_{dist}), and kurtosis (K_{dist}).

2.2.1. Two-Parameter Weibull (WEI) Distribution

The probability density function (PDF) $f_{\mathrm{WEI}}(x)$ and the cumulative distribution function (CDF) $F_{\mathrm{WEI}}(x)$ for the WEI distribution are defined as follows [41,42]:

$$f_{\mathrm{WEI}}(x) = \frac{\alpha}{\beta^{\alpha}} x^{\alpha-1} e^{\left(-\left(\frac{x}{\beta}\right)^{\alpha}\right)}, \; F_{\mathrm{WEI}}(x) = 1 - e^{\left(-\left(\frac{x}{\beta}\right)^{\alpha}\right)} \tag{1}$$

for $x > 0, \alpha > 0, \beta > 0$, where α is the dimensionless shape parameter, and β is the scale parameter in the units of the wind speed. Table 1 summarizes the statistical properties (SPs) of the WEI distribution.

Table 1. Statistical properties of the WEI distribution [20,43].

SP	Expression
$\overline{v}_{dist}$	$\beta\Gamma\left(1+\alpha^{-1}\right)$
${\sigma^2}_{dist}$	$\beta^2\left[\Gamma\left(1+2\alpha^{-1}\right)-\Gamma^2\left(1+\alpha^{-1}\right)\right]$
μ_3	$\beta^3\Gamma\left(1+3\alpha^{-1}\right)$
S_{dist}	$\frac{\Gamma\left(1+3\alpha^{-1}\right)-3\Gamma\left(1+2\alpha^{-1}\right)\Gamma\left(1+\alpha^{-1}\right)+2\Gamma^3\left(1+\alpha^{-1}\right)}{\left[\Gamma\left(1+2\alpha^{-1}\right)-\Gamma^2\left(1+\alpha^{-1}\right)\right]^{3/2}}$
K_{dist}	$\frac{\Gamma\left(1+\frac{4}{\alpha}\right)-4\Gamma\left(1+\frac{3}{\alpha}\right)\Gamma\left(1+\frac{1}{\alpha}\right)+6\Gamma\left(1+\frac{2}{\alpha}\right)\Gamma^2\left(1+\frac{1}{\alpha}\right)-3\Gamma^4\left(1+\frac{1}{\alpha}\right)}{\left[\Gamma\left(1+\alpha^{-1}\right)-\Gamma^2\left(1+\alpha^{-1}\right)\right]^2}$

2.2.2. Rayleigh (RAY) Distribution

The RAY distribution is a special case of the WEI distribution with $\alpha = 2$, leading to the PDF $f_{\mathrm{RAY}}(x)$ and CDF $F_{\mathrm{RAY}}(x)$ in Equation (2), as follows [31,44]:

$$f_{\mathrm{RAY}}(x) = x\sigma^{-2}e^{-0.5\left(\frac{x}{\sigma}\right)^2},\ F_{\mathrm{RAY}}(x) = 1 - e^{-0.5\left(\frac{x}{\sigma}\right)^2} \tag{2}$$

Table 2 summarizes the SPs of the RAY distribution.

Table 2. Statistical properties of the RAY distribution [20].

SP	Expression
$\overline{v}_{dist}$	$\sigma\sqrt{\frac{\pi}{2}}$
${\sigma^2}_{dist}$	$\left(\frac{4-\pi}{2}\right)\sigma^2$
μ_3	$3.76\sigma^3$
S_{dist}	$\frac{(-3+\pi)\sqrt{\frac{\pi}{2}}}{\left(2-\frac{\pi}{2}\right)^{3/2}}$
K_{dist}	$\frac{32-3\pi^2}{(4-\pi)^2}$

2.2.3. Two-Parameter Gamma (GAM) Distribution

The PDF $f_{\mathrm{GAM}}(x)$ and the CDF $F_{\mathrm{GAM}}(x)$ of the GAM distribution are given by Equation (3) [27,30].

$$f_{\mathrm{GAM}}(x) = \frac{x^{\alpha-1}}{\beta^{\alpha}\Gamma(\alpha)}e^{\left(-\frac{x}{\beta}\right)},\ F_{\mathrm{GAM}}(x) = \frac{\Gamma_{x/\beta}(\alpha)}{\Gamma(\alpha)} \tag{3}$$

for $x > 0, \alpha > 0, \beta > 0$, where $\Gamma(\alpha) = \int_0^{\infty} t^{\alpha-1}e^{-t}dt\ (\alpha > 0)$ is the Gamma function, and $\Gamma_x(\alpha) = \int_0^{x} t^{\alpha-1}e^{-t}dt\ (\alpha > 0)$ is the incomplete Gamma function. α is the shape parameter, while β is the scale parameter. Table 3 outlines the SPs of the GAM distribution.

Table 3. Statistical properties of the GAM distribution [20,43].

SP	Expression
$\overline{v}_{dist}$	$\beta\alpha$
${\sigma^2}_{dist}$	$\alpha\beta^2$
μ_3	$\alpha^3\beta(\beta+2)(\beta+1)$
S_{dist}	$\frac{2\beta^2}{\alpha}$
K_{dist}	$3+\frac{6}{\alpha}$

2.2.4. Generalized Extreme Value (GEV) Distribution

The PDF $f_{\mathrm{GEV}}(x)$ and the CDF $F_{\mathrm{GEV}}(x)$ of the GEV distribution are given by Equation (4) [23,28,45].

$$f_{\mathrm{GEV}}(x) = \frac{1}{\sigma} \mathrm{e}^{[-(1+kz)^{-1/k}]} (1+kz)^{-1-1/k},\ F_{\mathrm{GEV}}(x) = \mathrm{e}^{[-(1+kz)^{-1/k}]} \tag{4}$$

for $k \neq 0, 1 + k\frac{(x-\mu)}{\sigma} > 0$, where $z \equiv \frac{x-\mu}{\sigma}$. k is the shape parameter, σ is the scale parameter, and μ is the location parameter. Table 4 gives the SPs of the GEV distribution.

Table 4. Statistical properties of the GEV distribution [43].

SP	Expression
$\overline{v}_{dist}$	$\mu - \frac{\sigma}{k}(1 - \Gamma(1-k))$
${\sigma^2}_{dist}$	$\frac{\sigma^2}{k^2}\left(\Gamma(1-2k) - \left(\Gamma(1-k)\right)^2\right)$
μ_3	$\frac{1}{k^3}\left[(\mu k - \sigma)^3 + \sigma^3\Gamma(1-3k) + 3(\mu k - \sigma)\sigma(\sigma\Gamma(1-2k) + (\mu k - \sigma)\Gamma(1-k))\right]$
S_{dist}	$\frac{k}{\lvert k\rvert}\frac{\Gamma(1-3k) - 3\Gamma(1-2k)\Gamma(1-k) + 2\left(\Gamma(1-k)\right)^3}{\left(\Gamma(1-2k) - (\Gamma(1-k))^2\right)^{3/2}}$
K_{dist}	$\frac{\Gamma(1-4k) - 4\Gamma(1-3k)\Gamma(1-k) + 6\Gamma(1-2k)\left(\Gamma(1-k)\right)^2 - 3\left(\Gamma(1-k)\right)^4}{\left(\Gamma(1-2k) - (\Gamma(1-k))^2\right)^2}$

2.2.5. Two-Parameter Inverse Gaussian (IGA) Distribution

The PDF $f_{\mathrm{IGA}}(x)$ and the CDF $F_{\mathrm{IGA}}(x)$ of the IGA distribution are given by Equation (5) [19,28,32].

$$f_{\mathrm{IGA}}(x) = \sqrt{\frac{\lambda}{2\pi x^3}} e^{\left(-\frac{\lambda(x-\mu)^2}{2\mu^2 x}\right)},\ F_{\mathrm{IGA}}(x) = \Phi\left(\sqrt{\frac{\lambda}{x}}\left(\frac{x}{\mu} - 1\right)\right) + \Phi\left(-\sqrt{\frac{\lambda}{x}}\left(\frac{x}{\mu} + 1\right)\right) e^{\left(\frac{2\lambda}{\mu}\right)} \tag{5}$$

for $x > 0, \mu > 0, \lambda > 0$, where $\Phi(x) = \frac{1}{\sqrt{2\pi}} \int_0^x e^{-t^2/2} dt$ is the Laplace integral. Table 5 summarizes the SPs of the IGA distribution, where λ is the shape parameter, and μ is the scale parameter.

Table 5. Statistical properties of the IGA distribution [43].

SP	Expression
$\overline{v}_{dist}$	μ
${\sigma^2}_{dist}$	$\frac{\mu^3}{\lambda}$
μ_3	$\frac{3\mu^5}{\lambda^2} + \frac{3\mu^4}{\lambda} + \mu^3$
S_{dist}	$3\sqrt{\frac{\mu}{\lambda}}$
K_{dist}	$3 + 15\frac{\mu}{\lambda}$

2.2.6. Gumbel Distribution (GUM)

The PDF $f_{\mathrm{GUM}}(x)$ and the CDF $F_{\mathrm{GUM}}(x)$ of the GUM distribution are given by Equation (6) [23,46].

$$f_{\mathrm{GUM}}(x) = \frac{1}{\beta} e^{(-z - e^{(-z)})},\ F_{\mathrm{GUM}}(x) = e^{(-e^{(-z)})} \tag{6}$$

for $x > 0,\ \beta > 0$, where $z \equiv \frac{x-\mu}{\beta}$. β is the scale parameter, and μ is the location parameter. Table 6 summarizes the SPs of the GUM distribution.

Table 6. Statistical properties of the GUM distribution [43].

SP	Expression
$\overline{v}_{dist}$	$\mu + \gamma\beta$ where γ is the Euler–Mascheroni constant = 0.577215
${\sigma^2}_{dist}$	$\frac{\pi^2}{6}\beta^2$
μ_3	$\mu^3 + 3\gamma\mu^2\beta + 3\left(\frac{\pi^2}{6} + \gamma^2\right)\mu\beta^2 - \left(\frac{\pi^2}{3} - \frac{\pi^2}{6}\gamma + 2\gamma^3 + \gamma^2 - 2\zeta(3)\right)\beta^3$ where $\zeta(3)$ is the Riemann zeta function at 3 = 1.202057
S_{dist}	$\frac{12\sqrt{6}}{\pi^3}\zeta(3) = 1.202057$
K_{dist}	$\frac{12}{5} = 2.4$

2.3. Methods for Estimating Distribution Parameters

Maximum Likelihood Method (MLM)

The present study utilizes the maximum likelihood method (MLM) to estimate the parameters of the six distributions (GAM, GEV, GUM, IGA, RAY, WEI), with the specific form of $f(x;\theta)$ varying according to the chosen distribution [23,47]. The MLM method was chosen for parameter estimation due to its efficiency and accuracy in fitting the distributions to wind speed data [28]. MLM is a widely accepted approach, as it minimizes the mean squared error and ensures the best possible alignment between the data and the probability distribution function [31]. Given the challenge of accurately determining the parameters of distributions, MLM provides a reliable estimation compared to other methods [48].

The general form of the maximum likelihood method (MLM) method for estimating the parameters $\theta = (\theta_1, \theta_2, \ldots, \theta_m)$ of a wind speed distribution is given as follows.

For wind speed data $\{x_1, x_2, \ldots, x_n\}$, the log-likelihood function is as follows:

$$l(\theta) = \sum_{i=1}^{n} \log f(x_i;\theta) \tag{7}$$

where $f(x_i;\theta)$ is the probability density function (PDF) of the respective distribution.

The aim is to minimize the negative log-likelihood function, as follows:

$$-l(\theta) = -\sum_{i=1}^{n} \log f(x_i;\theta) \tag{8}$$

The optimal parameters $\hat{\theta}$ are obtained by solving the following:

$$\frac{\partial l(\theta)}{\partial \theta} = 0 \tag{9}$$

using numerical optimization techniques such as the limited-memory Broyden–Fletcher–Goldfarb–Shanno with box constraints (L-BFGS-B), Nelder–Mead, and Newton–Raphson methods [26,30,49,50]. Python scripts (version 3.9.12) were implemented to carry out the optimization and estimate the parameters.

2.4. Goodness-of-Fit Test of Stastical Distributions

The distribution that best represents the observed data is obtained by performing the goodness-of-fit test. A well-fitted model effectively captures the detailed features of the observed data, facilitating the estimation of parameters of the distribution model with minimal uncertainty, precisely depicting data variability, and enhancing confidence in predicting new observations. In this study, the following three test statistics were utilized: the Kolmogorov–Smirnov (KSS) test, the Anderson–Darling (AD) test, and the

wind power density error (WPDE). The AD test assigns greater significance to deviations in the distribution tails. In contrast, the KSS test is more sensitive to differences near the center of the distribution curve, and the WPDE assesses discrepancies specifically related to wind power density. Since each performance statistical indicator can yield varying results, a parameter known as the total error (TE) was utilized to rank the distributions based on their accuracy [45].

2.4.1. Kolmogorov–Smirnov (KSS) Test

The KSS is given by the following equation [51]:

$$\mathrm{KSS} = \max|\mathrm{E(x)} - \mathrm{T(x)}| \tag{10}$$

where $\mathrm{E(x)}$ denotes the empirical CDF and $\mathrm{T(x)}$ denotes the theoretical CDF. A lower KSS statistic signifies a closer match between the theoretical and empirical distribution functions.

2.4.2. Anderson–Darling (AD) Test

The AD test, a refinement of the KSS test, is frequently used to evaluate goodness-of-fit. The AD test statistic is computed using Equation (10) [31]:

$$A^2 = -n - \frac{\sum_{j=1}^{n}(2j-1)}{n}\left[\ln \mathrm{G}(x_j) + \ln\left(1 - \mathrm{G}(x_{n-j+1})\right)\right] \tag{11}$$

where $\mathrm{G}(x_j)$ represents the cumulative distribution function (CDF) of the tested probability density function (PDF). Similar to the KSS test, a lower AD test statistic indicates a better fit of the theoretical distribution model.

2.4.3. Wind Power Density Error (WPDE)

The WPDE was also utilized to evaluate the performance of each method of estimating the wind power density [52]. The WPDE is given in the following equation [53]:

$$\mathrm{WPDE} = \left| \frac{\mathrm{WPD_{i,dis}} - \mathrm{WPD_{i,obs}}}{\mathrm{WPd_{i,obs}}} \right| \tag{12}$$

where $\mathrm{WPD_{i,obs}}$ represents the wind power density calculated using actual data, and $\mathrm{WPD_{i,dis}}$ represents the wind power density calculated from the distribution function.

2.4.4. Total Error (TE)

TE evaluates the performance of statistical distributions by averaging normalized statistical indicators or metrics [45]. This study utilized three indicators: KSS, AD, and WPDE. Each statistic was normalized using Equation (13):

$$X_{\mathrm{norm}} = \frac{X - X_{\mathrm{min}}}{X_{\mathrm{max}} - X_{\mathrm{min}}} \tag{13}$$

where X represents the metric value, and X_{min} and X_{max} are its minimum and maximum values, respectively. This normalization scales the statistic between 0 and 1 for comparability.

The TE is then calculated using Equation (14):

$$TE = \frac{KS_{\mathrm{norm}} + AD_{\mathrm{norm}} + WPDE_{\mathrm{norm}}}{3} \tag{14}$$

This provides a composite score reflecting each distribution's overall fit and accuracy.

2.5. Wind Direction Analysis

The primary function of a wind rose is to present data on wind speed and direction occurrences [54,55]. This information is crucial for site selection, as it helps identify the optimal locations for installing wind turbines to maximize wind power utilization [56]. In this study, the wind direction measurements were clockwise, with the north as the reference point at zero degrees. The polar diagram of the wind rose was divided into 16 sectors, each spanning 22.5 degrees [57,58]. This study used the Windographer 4.0 software to generate a wind rose diagram with 16 sectors.

2.6. Wind Power Density Calculations

The wind power density for the observed data (WPD_{obs}) is given by Equation (15) [59], and the wind power densities for each distribution are given in Table 7.

$$WPD_{obs} = 0.5n^{-1}\rho\sum_{i=1}^{n} v_i^3 \quad (15)$$

Table 7. Wind power density (WPD) formula for each distribution.

Distribution	Wind Power Density for Each Distribution
WEI	$WPD_{WEI} = 0.5\rho c^3\Gamma\left(1+3\alpha^{-1}\right)$
RAY	$WPD_{RAY} = 0.5\rho\cdot 3.76\sigma^3$
GAM	$WPD_{GAM} = 0.5\rho\alpha^3\beta(\beta+2)(\beta+1)$
GEV	$WPD_{GEV} = 0.5\rho\frac{1}{k^3}\left[(\mu k-\sigma)^3+\sigma^3\Gamma(1-3k)+3(\mu k-\sigma)\sigma(\sigma\Gamma(1-2k)+(\mu k-\sigma)\Gamma(1-k))\right]$
IGA	$WPD_{IGA} = 0.5\rho\frac{3\mu^5}{\lambda^2}+\frac{3\mu^4}{\lambda}+\mu^3$
GUM	$WPD_{GUM} = 0.5\rho\mu^3+3\gamma\mu^2\beta+3\left(\frac{\pi^2}{6}+\gamma^2\right)\mu\beta^2-\left(\frac{\pi^2}{3}-\frac{\pi^2}{6}\gamma+2\gamma^3+\gamma^2-2\zeta(3)\right)\beta^3$ where $\zeta(3)$ is the Riemann zeta function at 3 = 1.202057

The wind power density was divided into seven categories based on the annual mean wind speed and power density, as shown in Table 8, which was used in this study to classify the wind resource availability at the University of Fort Hare at a height of 10 m above ground level (AGL).

Table 8. Wind resource availability classification [60–63].

Wind Power Class	Mean Wind Speed (m/s)	Wind Power Density (W/m^2)
1 (Poor)	0–4.4	0–100
2 (Marginal)	4.4–5.1	100–500
3 (Moderate)	5.1–5.6	200–250
4 (Good)	5.6–6.0	200–250
5 (Excellent)	6.0–6.4	250–300
6 (Excellent)	6.4–7.0	300–400
7 (Excellent)	7.0–9.4	400–1000

3. Results and Discussion

3.1. Descriptive Statistics of the Wind Speed

Table 9 presents the annual and monthly wind speed statistics for the University of Fort Hare, detailing the data size (N), range (R), mean wind speed ($\overline{v}_{obs}$), variance ($\sigma^2{}_{obs}$) standard deviation (σ_{obs}), coefficient of variation (CoV), skewness (S), kurtosis (K), and the minimum (Min) and maximum (Max) wind speeds based on the observed data. The mean

wind speed ($\overline{v}_{obs}$) peaked in July at 13.8m/s and was lowest in February at 8.3m/s. The observed σ^2_{obs} ranged from 2.119 in May to 2.872 in September, indicating fluctuations in wind speed consistency. The standard deviation (σ_{obs}) generally showed similar trends, with the highest values in July (4.83 m/s) and lowest values in May (2.44 m/s). The variability in the wind speeds across the months demonstrated significant fluctuations, as the CoV values indicate. In July, the wind speed variability was at its peak, with a CoV of 77%, marking it as the most unpredictable month. This was followed by May and August, each with a CoV of 74%, reflecting similarly extreme variability [19,34]. Conversely, January and September exhibited relatively lower CoV values of 63% and 67%, respectively, though still above the threshold for high variability (>40%) [64]. The positive skewness suggests that the measured wind speeds were typically above the mean, indicating better wind performance at this location and a right-skewed distribution [1,34]. These results are similar to other studies [29,64]. The kurtosis values were positive and less than 3, except in January. The maximum wind speed recorded was 13.8 m/s, reflecting a steady upper limit across the observations. Overall, these results indicate clear seasonal variation in wind characteristics, with notable mid-year peaks and a general trend of increasing variability during the summer months.

Table 9. Annual and monthly statistical wind data for University of Fort Hare at 10 m AGL.

Month	N	R	$\overline{v}_{obs}$	$\sigma^2{}_{obs}$	σ_{obs}	CoV(%)	S	K	Min	Max
Jan	2232	9.5	2.756	3.04	1.74	63	0.59	−0.04	0	9.5
Feb	2016	8.3	2.481	3.12	1.77	71	0.71	0.09	0	8.3
Mar	2232	9.5	2.456	2.94	1.72	70	0.87	0.63	0	9.5
Apr	2160	9.6	2.234	2.48	1.57	70	1.12	1.61	0	9.6
May	2232	11.5	2.119	2.44	1.56	74	1.52	3.69	0	11.5
Jun	2160	11.1	2.653	3.57	1.89	71	1.39	2.09	0	11.1
Jul	2232	13.8	2.848	4.83	2.20	77	1.58	2.61	0	13.8
Aug	2232	12.0	2.710	3.97	1.99	74	1.36	2.10	0	12.0
Sept	2160	10.6	2.872	3.67	1.92	67	1.15	1.48	0	10.6
Oct	2232	10.9	2.762	3.61	1.90	69	0.76	0.43	0	10.9
Nov	2160	9.4	2.669	3.32	1.82	68	0.63	0.05	0	9.4
Dec	2232	10.2	2.670	3.46	1.86	70	0.74	0.32	0	10.2
Annual	26,280	13.8	2.603	3.42	1.85	71	1.12	1.56	0	13.8

As illustrated in Figure 3, the monthly mean wind speed values typically ranged from 2.6 to 2.9 m/s, with only a few instances falling below 2.4 m/s. The highest monthly mean value, 2.872 m/s, was recorded in September.

Figure 4 depicts a comparison of four statistical metrics, namely, the mean, variance, skewness, and kurtosis, across the six distributions (GAM, GEV, GUM, IGA, WEI, RAY) relative to the actual wind data. The actual wind data's mean was 2.603 m/s, which was closely approximated by most distributions with minimal variation. The GEV distribution had the closest mean of 2.602 m/s. The actual data had a variance of 3.424. However, the variance of the distributions showed more variation, indicating differences in data spread. The GEV distribution closely matched this variance with a value of 3.447, while the GAM distribution deviated the most, showing a significantly lower variance of 2.365. The skewness of the actual data was 1.12, a positive value, and the skewness values calculated from all the distributions were also positive. The GEV distribution, with a skewness of 1.28, and the GUM distribution, with a skewness of 1.14, were closer to the actual data, while the IGA distribution exhibited the highest skewness at 1.675, indicating a more pronounced right-skewed distribution. The GAM distribution, on the other hand, had the lowest skewness at 0.366, indicating less asymmetry than the actual data. In terms

of kurtosis, the actual data showed a value of 1.57, suggesting that the wind speed data had few extreme values. The GEV distribution exhibited a kurtosis of 6.14, which was significantly higher than the kurtosis of the actual wind data, indicating a more pronounced peak and steeper tails. The IGA distribution demonstrated an even higher kurtosis of 7.68, suggesting an exceptionally sharp peak. Also, the GUM, GAM, WEI, and RAY distributions showed kurtosis values that were also higher than the actual wind data but not as extreme as the IGA and GEV distributions. While most of the distributions aligned reasonably well with the actual wind data in terms of mean and variance, the IGA and GEV distributions deviated the most in their kurtosis, highlighting their tendency for sharper peaks and heavier tails. The results also showed a similar trend to the findings of [43], where the distributions exhibited variations in these statistical properties compared to the values obtained from actual wind speed data, especially when the parameters were estimated using the maximum likelihood method.

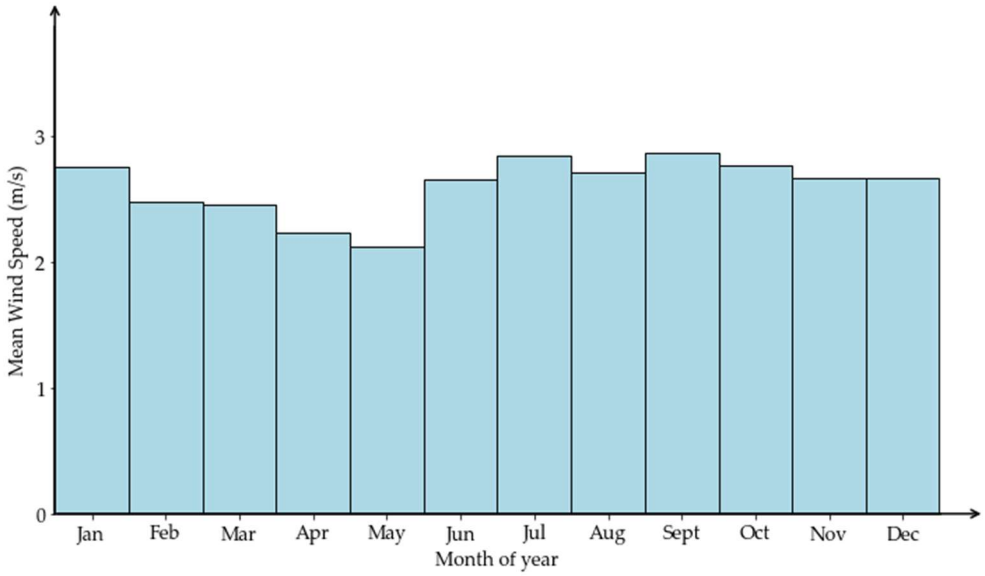

Figure 3. Monthly average wind speed at 10m AGL for the University of Fort Hare.

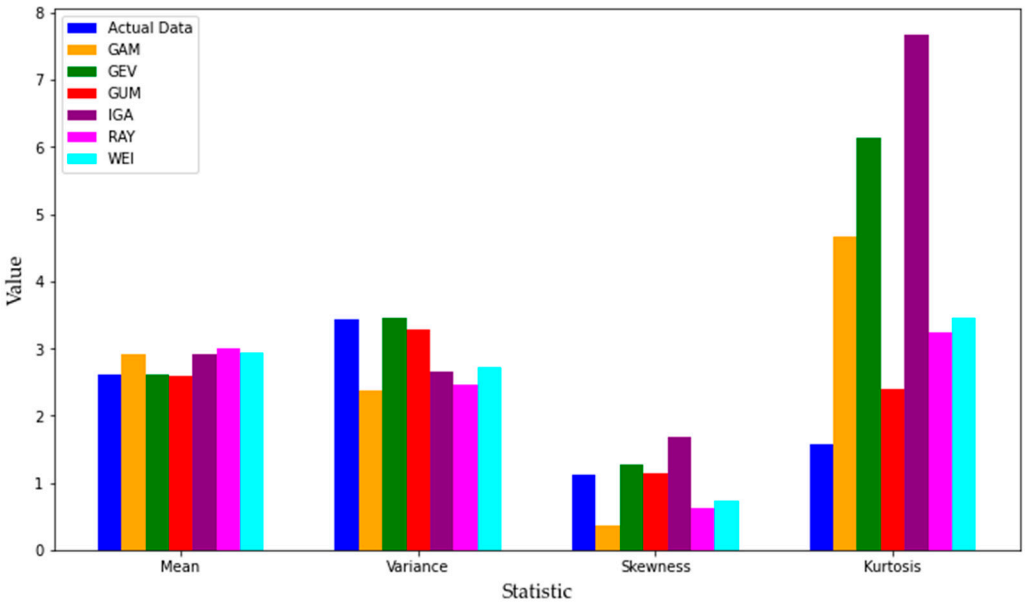

Figure 4. Comparison of statistical metrics for the six distributions.

The diurnal variation in the mean wind speed, as shown in Figure 5, illustrated a clear daily cycle over a 24 h period. During the early morning hours, from midnight to around 8 a.m., the wind speeds were relatively low and remained almost constant. At around 8:30 a.m., the wind speed began to increase gradually, followed by a sharp rise after 9:00 a.m., peaking in the late afternoon at 5 p.m. with a maximum value of 4.28 m/s. After this peak, the wind speeds steadily declined as the day transitioned into evening, reaching a minimum of 1.65 m/s early at 8 a.m. The dome-shaped profile shown in the Figure 5 indicates that the Fort Hare area experienced windy conditions from mid-morning to early evening, consistent with the findings of [34].

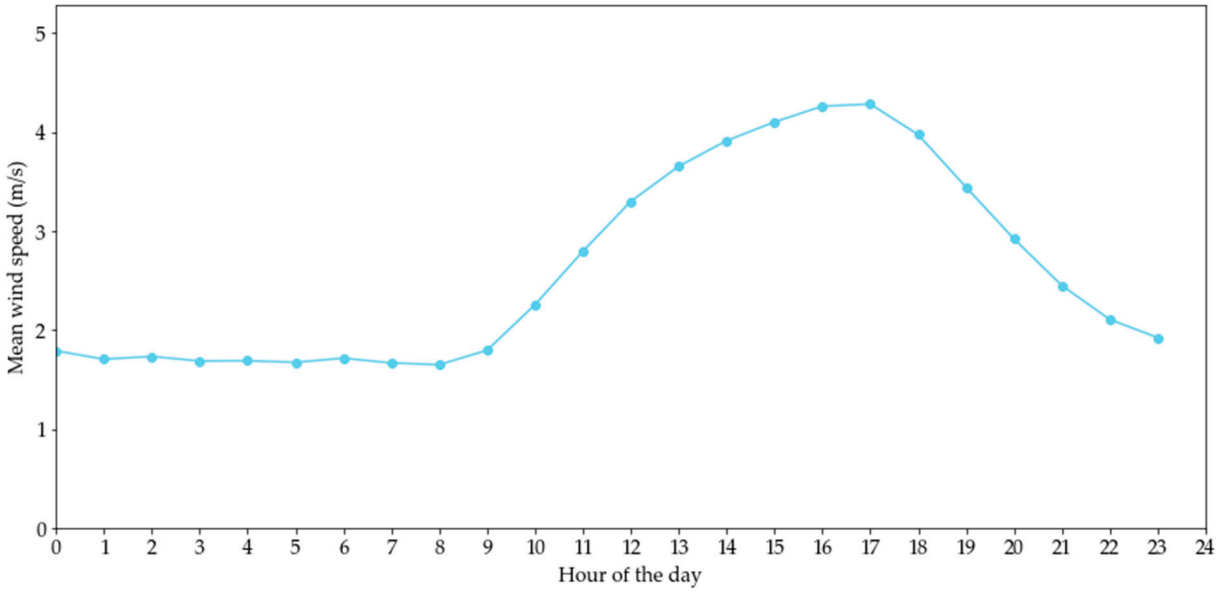

Figure 5. Diurnal variation in mean wind speed at the University of Fort Hare.

A further analysis of the seasonal statistical wind speed data is depicted in Table 10. Winter showed the highest maximum wind speed at 13.8 m/s and the greatest variability, with a standard deviation of 2.03 m/s and the highest skewness, S = 1.48, indicating more high-speed outliers. Autumn had a moderate maximum speed of 11.5 m/s but exhibited the highest kurtosis, K = 1.77, suggesting a more pronounced peak around the mean. Summer and spring displayed similar patterns, with lower mean wind speeds and variability, as indicated by the lower coefficients of variation, CoV = 0.68, suggesting more consistent wind speeds during these seasons. This seasonal variability and distributional shape offer valuable insights into the wind behaviour annually.

Table 10. The seasonal statistical wind data for University of Fort Hare at 10 m AGL.

Season	N	R	$\overline{v}_{obs}$	${\sigma^2}_{obs}$	σ_{obs}	CoV	S	K	Min	Max
Summer	6480	10.2	2.641	3.22	1.79	0.68	0.68	0.14	0	10.2
Autumn	6624	11.5	2.270	2.64	1.62	0.72	1.15	1.77	0	11.5
Winter	6624	13.8	2.738	4.14	2.03	0.74	1.48	2.47	0	13.8
Spring	6552	10.9	2.768	3.54	1.88	0.68	0.86	0.74	0	10.9

3.2. Analysis of Probability Distribution Functions

The parameters of the six distribution functions, estimated using the seasonal and overall wind speed data, are presented in Table 11.

Table 11. Probability distribution function parameters.

Season	Distribution	Parameters
Summer	GAM	α = 3.87196207204796 β = 0.77507456427451
	GEV	k = −0.056960272557 σ = 1.4972487444338 μ = 1.848955588234
	GUM	β = 1.4709535966597 μ = 1.8035050553625
	IGA	λ = 9.9954369211484 μ = 3.0010579509349
	RAY	σ = 2.4065996370416
	WEI	α = 2.0109418096457 β = 3.4078140596928
Autumn	GAM	α = 3.9885106615485 β = 0.6490508105913
	GEV	k = 0.0092984086461 σ = 1.2467280783248 μ = 1.5389917873736
	GUM	β = 1.2502151454179 μ = 1.5383209018954
	IGA	λ = 9.6627572702393 μ = 2.5888085399449
	RAY	σ = 2.1079513803782
	WEI	α = 1.9027909814916 β = 2.9407369404527
Winter	GAM	α = 3.16024334329771 β = 0.9410806487361
	GEV	k = 0.0992291628189 σ = 1.3671470841441 μ = 1.7981664820307
	GUM	β = 1.4179032191099 μ = 1.8725161930694
	IGA	λ = 8.5461048436524 μ = 2.9740444076619
	RAY	σ = 2.5135424855173
	WEI	α = 1.6904507406495 β = 3.3661889532314
Spring	GAM	α = 3.7247001946047 β = 0.8304135151953
	GEV	k = -0.023269024722 σ = 1.5140912691744 μ = 1.9235752478768
	GUM	β = 1.5031457206771 μ = 1.9046835216656
	IGA	λ = 9.9870434393496 μ = 3.0930411052362
	RAY	σ = 2.5016406862587
	WEI	α = 1.9406039977847 β = 3.5111781389429
Overall	GAM	α = 3.5927533461899 β = 0.8113562688486
	GEV	k = 0.0226298979109 σ = 1.4040697074707 μ = 1.7591867818483
	GUM	β = 1.4442754819722 μ = 1.7706426185743
	IGA	λ = 9.3517654063929 μ = 2.9150050416826
	RAY	σ = 2.3898368796538
	WEI	α = 1.8510621376527 β = 3.3081271593922

The corresponding seasonal and overall wind speed distribution graphs illustrate how well the fitted probability density functions represent the observed data, as shown in Figures 6 and 7. As indicated in Figure 6, the GEV distribution provided the best fit for the entire period, aligning closely with the histogram's peak between 1 and 2 m/s and the tails, effectively modeling infrequent higher wind speeds beyond 8 m/s. GUM, ranked second, followed closely, while RAY, ranked last, failed to capture the central tendency and distribution spread.

Seasonally, as shown in Figure 7, the GEV distribution consistently performed the best across all seasons, excelling in capturing peaks and tails. GUM ranked second in all seasons. In summer, IGA ranked last. RAY struggles in autumn and winter, ranking last in both seasons, while GAM consistently ranked fifth in all seasons except for spring, where it ranked fourth. GAM failed to effectively represent the variability and extreme wind patterns. These results confirm the GEV distribution's robustness in modeling wind speed patterns across different periods. However, it is important to note that the GEV distribution, having three parameters compared to the other distributions with one or two parameters, involves more complex parameter estimation methods. This complexity often leads to a preference for distributions that offer simpler estimation methods, particularly the widely used Weibull distribution [28].

The fitting of the distributions to the actual wind speed data is also validated by the goodness-of-fit test results, as shown in Table 12 for the four seasons and in Table 13 for the entire period of 2021–2023.

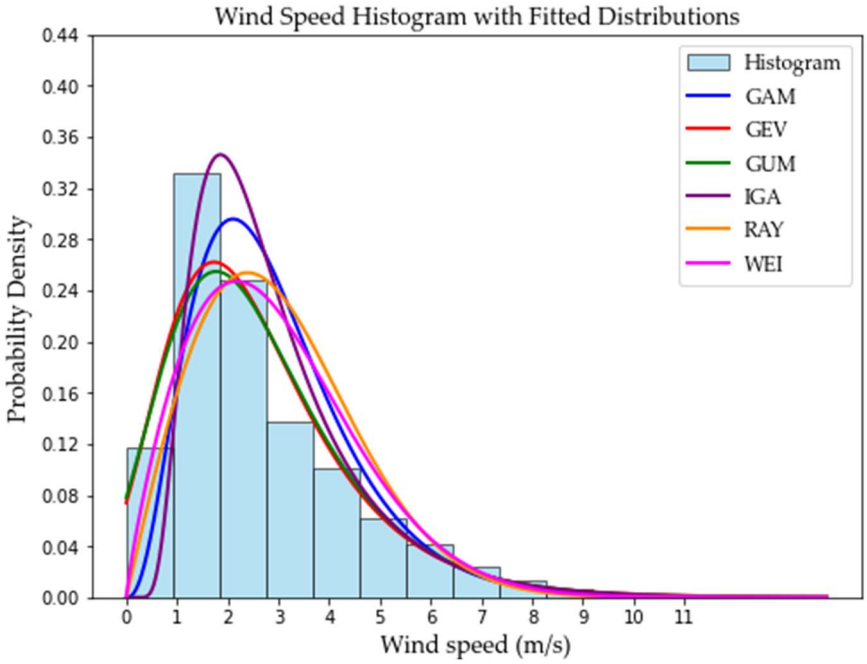

Figure 6. Weibull distributions fitted to the observed data histogram for 2021–2023.

Table 12. Performance comparison of the six distributions for the four seasons.

	Distribution	KSS	Rank	AD	Rank	WPDE	Rank	TE	Overall Rank
Summer	GAM	0.160	6	1304.12	5	0.078	2	0.752	5
	GEV	0.083	1	49.31	1	0.012	1	0.000	1
	GUM	0.087	2	53.63	2	0.264	6	0.351	2
	IGA	0.149	3	1310.79	6	0.226	5	0.901	6
	RAY	0.151	4	1250.36	3	0.095	4	0.723	3
	WEI	0.153	5	1258.62	4	0.093	3	0.732	4
Autumn	GAM	0.192	5	1404.10	5	0.059	5	0.650	5
	GEV	0.123	1	108.60	2	0.000	1	0.000	1
	GUM	0.123	2	107.55	1	0.367	6	0.336	2
	IGA	0.175	3	1389.97	4	0.012	2	0.537	3
	RAY	0.207	6	1445.22	6	0.017	3	0.682	6
	WEI	0.189	4	1357.59	3	0.032	4	0.601	4
Winter	GAM	0.182	5	1038.83	5	0.156	5	0.526	5
	GEV	0.116	2	101.15	1	0.054	1	0.022	1
	GUM	0.107	1	116.44	2	0.468	6	0.337	2
	IGA	0.163	3	1000.61	3	0.055	2	0.385	3
	RAY	0.240	6	1329.52	6	0.109	4	0.711	6
	WEI	0.173	4	1012.23	4	0.065	3	0.422	4

Table 12. *Cont.*

	Distribution	KSS	Rank	AD	Rank	WPDE	Rank	TE	Overall Rank
Spring	GAM	0.151	6	1184.74	4	0.024	2	0.674	4
	GEV	0.079	1	45.54	1	0.017	1	0.000	1
	GUM	0.081	2	46.84	2	0.296	6	0.343	2
	IGA	0.145	4	1187.60	6	0.164	5	0.814	6
	RAY	0.150	5	1186.30	5	0.045	3	0.695	5
	WEI	0.139	3	1142.25	3	0.055	4	0.642	3

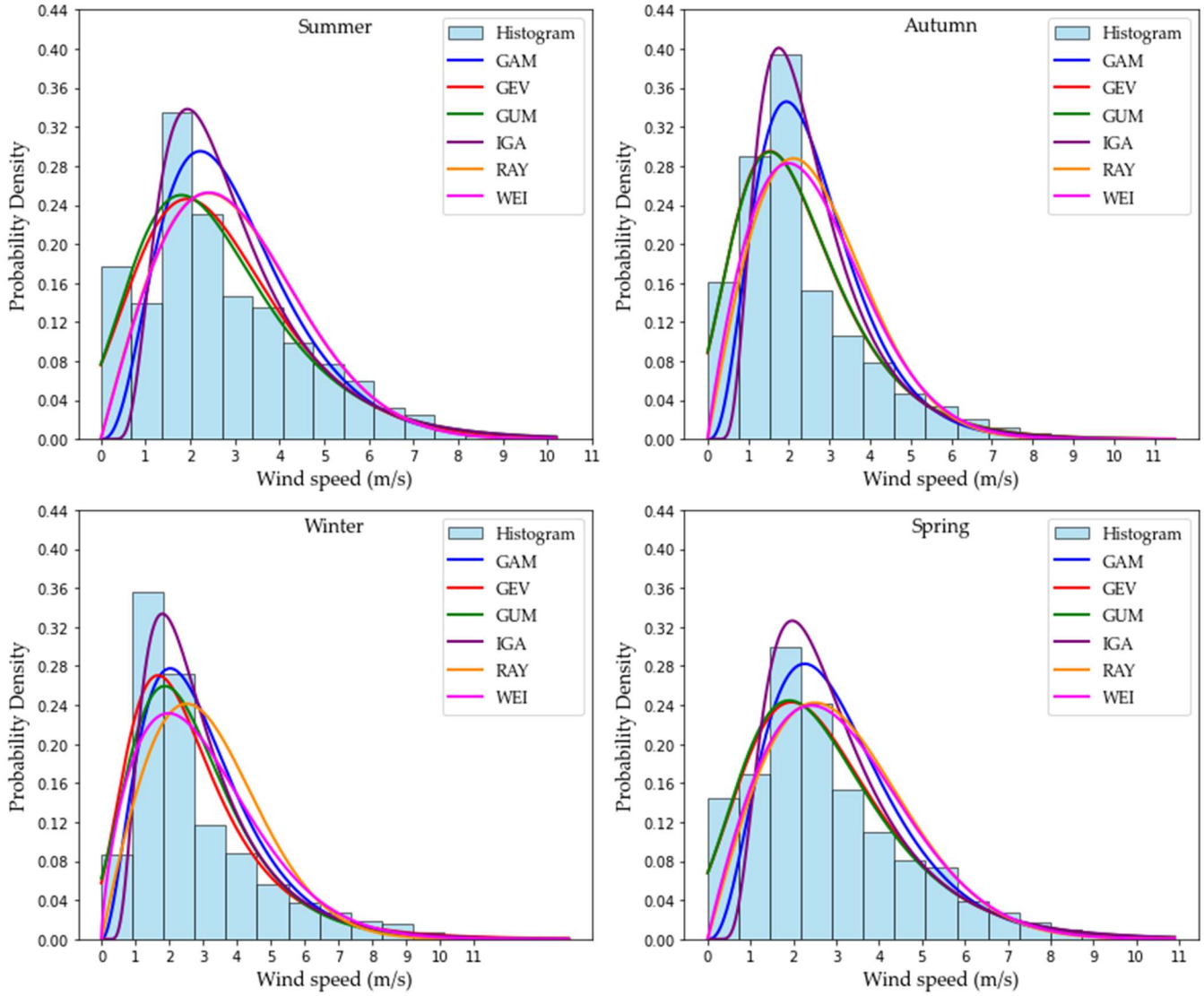

Figure 7. Histograms with fitted distributions for seasonal wind speed data.

As shown in Table 12, the GEV distribution consistently demonstrated the best performance across all seasons, as previously seen in Figure 7, with the lowest TE values: 0.00 in summer, 0.00 in autumn, 0.022 in winter, and 0.00 in spring. These values highlight the GEV distribution's superior ability to model the wind speed data effectively. In contrast, the IGA distribution ranked the worst, with the highest TE values of 0.90 in summer and 0.81 in winter, while the RAY distribution was also ranked last in autumn and winter, with TE values of 0.68 and 0.71, respectively. Notably, the dominance of the GEV distribution

remained consistent regardless of seasonal changes. The WEI distribution ranked fourth in summer, autumn, and winter and third in spring.

Table 13. Performance comparison of the six distributions for the entire period of 2021–2023.

Distribution	KSS	Rank	AD	Rank	WPDE	Rank	TE	Overall Rank
GAM	0.1699	5	4910.418	5	0.042	4	0.6005	5
GEV	0.0995	1	276.9513	2	0.024	3	0.0202	1
GUM	0.1012	2	272.8823	1	0.367	6	0.3394	2
IGA	0.1526	3	4868.478	4	0.072	5	0.5622	4
RAY	0.1917	6	5259.141	6	0.003	1	0.6667	6
WEI	0.1622	4	4735.565	3	0.022	2	0.5421	3

In Figure 8, the TE for each distribution listed in Table 13 is represented by individual bars, with different colors within each bar indicating the contribution of each normalized test statistic metric (KSS, AD, and WPDE) to the TE. Based on the analysis in Table 13 and Figure 8, which show the TE for each distribution, the GEV distribution emerged as the best-performing model, with the lowest TE of 0.0202, primarily influenced by the WPDE metric. Its three-parameter structure allowed it to capture rare and high-impact wind events, crucial for accurately representing variability in wind regimes. Additionally, it ranked first in KSS with a value of 0.0995, second in AD with 276.95, and third in WPDE with 0.024, demonstrating consistent performance across multiple indicators. The GUM distribution followed with a moderate TE of 0.3394, primarily driven by WPDE, as shown in Figure 8. The WEI distribution, with a TE of 0.5421, showed major contributions from KSS and AD. The IGA distribution had a TE of 0.5622, dominated by AD contributions, while the RAY distribution, with the highest TE of 0.6667, was mainly influenced by AD and KSS contributions. These findings align with the seasonal performance trends, confirming the GEV distribution as the most effective and robust model overall.

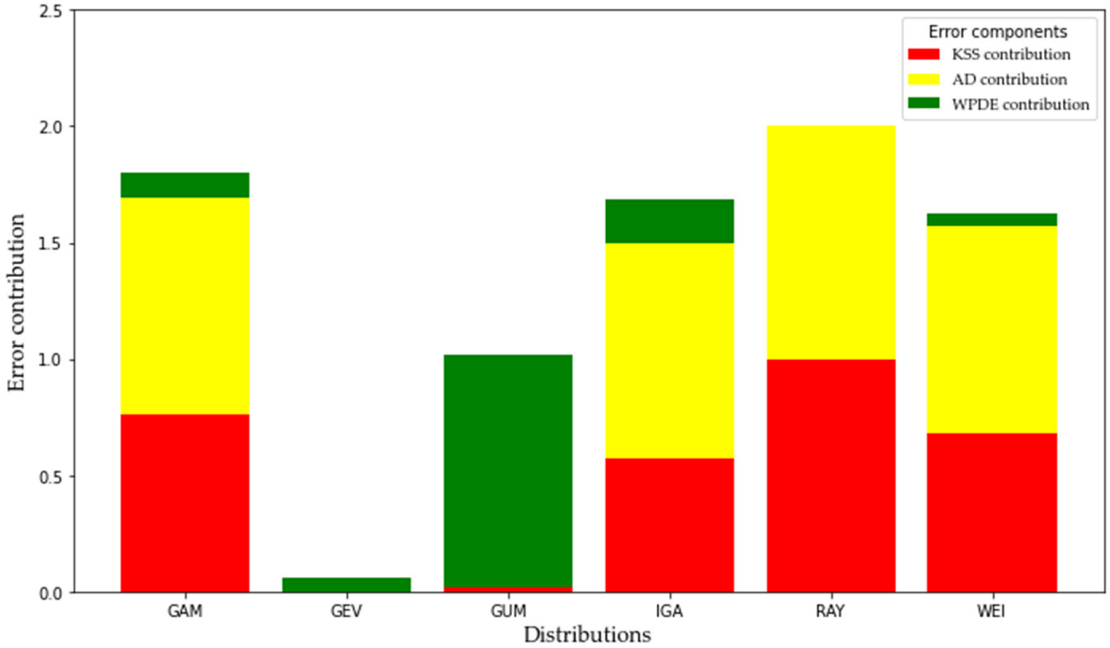

Figure 8. Contributions of normalized KSS, AD, and WPDE to TE for each distribution in Table 13.

It is worth noting that the RAY distribution performed poorly both seasonally and overall, further emphasizing its inadequacy. Its dismal performance can be attributed to its single-parameter structure, which assumes a zero mean wind vector an overly simplistic

approach that failed to capture the variability and extremes present in real-world wind speed data. Although the Weibull distribution ranked third out of six in this analysis, it remains a historically popular choice for wind speed modeling due to its simplicity and flexibility. Its two-parameter structure makes it easy to apply and compatible with various parameter estimation methods. For instance, the Weibull distribution, combined with the OpenWind method, has demonstrated notable effectiveness at sites such as Fort Beaufort and Upper Blinkwater in the Eastern Cape [1,4]. However, in this study, the GEV and GUM distributions, both designed to model extreme wind speeds, proved to be the most effective in fitting the wind data. Additionally, the performance of the Weibull distribution could potentially be improved using advanced optimization techniques, such as artificial intelligence, to refine its scale and shape parameter estimation.

3.3. Analysis of the Wind Power Density

The observed wind power density was measured as 31.52 W/m^2. In Table 14, the wind power density values for the different distributions, i.e., GAM, GEV, GUM, IGA, RAY, and WEI, ranged from 19.95 W/m^2 for GUM to 33.78 W/m^2 for IGA. Despite this range, all distributions fell into wind power class 1 (poor), indicating insufficient wind energy potential for large-scale electricity generation. When compared with the observed wind power density, measured at 31.52 W/m^2, the results were consistent, especially with the RAY distribution, which estimated a wind power density of 31.43 W/m^2. These similarities between the observed and modeled values further confirm that the site has limited suitability for wind energy development, as all values indicate poor wind power potential.

Table 14. Estimated wind power densities for the six distributions and their classification.

Distribution	WPD for Distribution (W/m^2)	Wind Power Class
GAM	30.19	1 (Poor)
GEV	32.29	1 (Poor)
GUM	19.95	1 (Poor)
IGA	33.78	1 (Poor)
RAY	31.43	1 (Poor)
WEI	32.20	1 (Poor)

It is, therefore, recommended that small-scale wind turbines for standalone applications be deployed at this site [24]. Notably, previous wind resource assessments in the Eastern Cape Province also suggested small-scale wind turbines for wind speeds measured at heights up to 30 m above ground level [1,7,34]. Additionally, greater wind energy can be captured by utilizing wind turbines with larger rotor diameters or by increasing the hub height [34]. On the other hand, augmentation systems (diffusers and concentrators) that enhance the wind speed at the rotor can be employed to enclose small-scale wind turbines, allowing them to operate effectively in the area under study [4,65].

3.4. Wind Direction Analysis

The wind directions were assessed for the entire study period and across the four seasons, as illustrated by the wind rose diagrams in Figures 9 and 10, respectively. Figure 9 highlights that the dominant wind direction for the 2021–2023 period was from the southeast, with the highest relative frequency of 16.35%. In contrast, winds from the northeast showed the lowest relative frequency, at just 0.4%. Identifying the prevailing wind direction is crucial for correctly orienting a wind turbine [36,42], which in this case should face southeast at Fort Hare University.

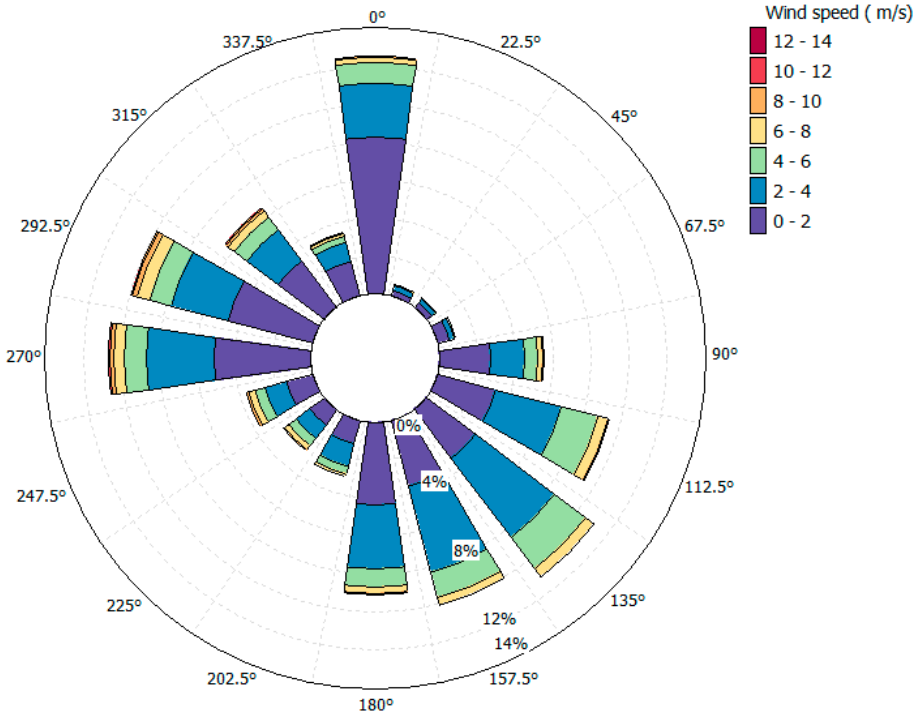

Figure 9. Wind rose diagram for overall wind direction for the 2021–2023 period.

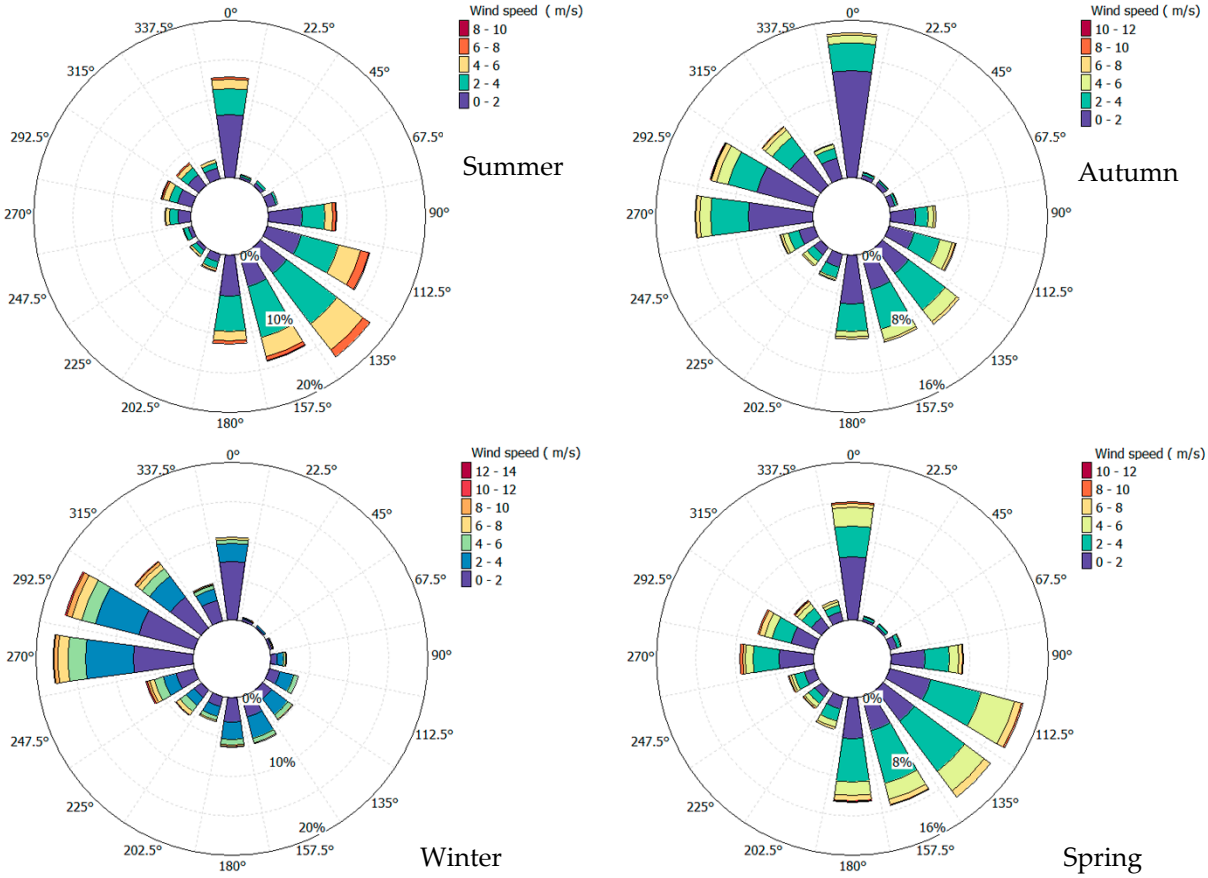

Figure 10. Wind rose diagram for seasonal wind direction variations for the 2021–2023 period.

The seasonal wind patterns shown in Figure 10 reveal that winds predominantly blow from the southeast during summer, spring, and autumn, aligning with the overall trend. However, winter winds primarily come from the northwest. A similar seasonal variation in

wind direction during winter was also observed by [34], where the winter wind direction diverged from the general pattern.

4. Conclusions

This study evaluated the wind energy potential at Fort Hare in the Eastern Cape, South Africa, using six statistical distribution models. It emphasizes the importance of selecting accurate models for wind energy estimation, moving beyond the traditional reliance on the two-parameter Weibull distribution. While the Weibull model is popular for its simplicity and flexibility, this study stresses the need for models tailored to a site's specific wind characteristics, which can vary over time and location.

A goodness-of-fit test approach was used, normalizing and averaging three statistical indicators to calculate the total error and rank model performance. This method, adapted from [45], was applied for the first time in wind potential assessments in the Eastern Cape. The comparison revealed that the generalized extreme value (GEV) distribution outperformed all the other models, accurately capturing wind speed variability and extremes, with the lowest total error being 0.020. In contrast, the Weibull and Rayleigh distributions recorded higher total errors of 0.5421 and 0.667, respectively, highlighting their limitations in representing highly variable wind data with extreme speeds. The Gumbel model also showed strong performance, confirming its applicability in similar environments. The GEV model was particularly effective in capturing seasonal wind speed variations and demonstrated consistent reliability across multiple goodness-of-fit indicators. These results highlight the importance of advanced statistical techniques in ensuring accurate wind power density estimations. Using the third moment for calculating wind power densities in models with more than two parameters could also improve accuracy.

The study classifies the site as having insufficient wind energy potential for large-scale electricity generation but recommends small-scale or augmented wind turbines for standalone systems. Additionally, turbines should be strategically placed in the southeast direction to maximize wind energy utilization, in alignment with prevailing wind patterns. These insights provide valuable guidance for optimizing wind resource utilization in South Africa and supporting sustainable energy development in areas with moderate wind potential.

While this study provides valuable insights into the wind energy potential at Fort Hare University, future research should focus on assessing wind characteristics at different heights above ground level, which is crucial for optimal wind turbine placement. Additionally, alternative methods such as Bayesian inference or metaheuristic algorithms could further enhance the accuracy of parameter estimation. Furthermore, future studies should integrate wind turbine power curves, techno-economic assessments, and advanced optimization techniques to improve wind energy potential assessments.

Author Contributions: Conceptualization, methodology, software, formal analysis, and writing—original draft preparation, N.S.; writing—review and editing, methodology, formal analysis, supervision, and funding acquisition P.M. and G.M. All authors have read and agreed to the published version of the manuscript.

Funding: This research received no external funding.

Institutional Review Board Statement: Not applicable.

Informed Consent Statement: Not applicable.

Data Availability Statement: The data presented in this study are available on request from the corresponding author.

Acknowledgments: Special acknowledgement is given to the National Research Foundation (NRF), Research Niche Area: Renewable Energy—Wind of GMRDC, University of Fort Hare for their financial support. The authors express their gratitude to South African Weather Services (SAWS) for providing data for this research at no cost.

Conflicts of Interest: The authors declare no conflicts of interest.

References

1. Shambira, N.; Makaka, G.; Mukumba, P.; Lesala, M.; Roro, K.; Julies, J.; Tazvinga, H. Wind Resource Assessment in the Upper Blinkwater Area in the Province of Eastern Cape, South Africa. *Int. J. Eng. Res. Technol.* **2020**, *9*, 387–402.
2. Ravanbach, B.; Kuhnel, M.; Hanke, B.; Von Maydell, K.; Van Dyk, E.E.; Vumbugwa, M.; Makaka, G.; Lesala, M.E.; Shambira, N.; Roro, K. Development of a Smart Monitoring and Evaluation Framework for Hybrid Renewable Mini-Grids. In Proceedings of the 2020 Fifteenth International Conference on Ecological Vehicles and Renewable Energies, EVER 2020, Monte-Carlo, Monaco, 10–12 September 2020.
3. Lesala, M.E.; Shambira, N.; Makaka, G.; Mukumba, P. Exploring Energy Poverty among Off-Grid Households in the Upper Blinkwater Community, South Africa. *Sustainability* **2024**, *16*, 4627. [CrossRef]
4. Shambira, N.; Makaka, G.; Mukumba, P. Velocity Augmentation Model for an Empty Concentrator-Diffuser-Augmented Wind Turbine and Optimisation of Geometrical Parameters Using Surface Response Methodology. *Sustainability* **2024**, *16*, 1707. [CrossRef]
5. Lesala, M.E.; Shambira, N.; Makaka, G.; Mukumba, P. The Energy Poverty Status of Off-Grid Rural Households: A Case of the Upper Blinkwater Community in the Eastern Cape Province, South Africa. *Energies* **2023**, *16*, 7772. [CrossRef]
6. Mukumba, P.; Chivanga, S.Y. An Overview of Renewable Energy Technologies in the Eastern Cape Province in South Africa and the Rural Households' Energy Poverty Coping Strategies. *Challenges* **2023**, *14*, 19. [CrossRef]
7. Tshimbiluni, H.C.; Tabakov, P.Y. Wind Energy Potential for Small-Scale WEC Systems in Port Elizabeth. In *IOP Conference Series: Earth and Environmental Science*; IOP Publishing: Bristol, UK, 2019; Volume 342.
8. Zhu, H.; Sueyoshi, M.; Hu, C.; Yoshida, S. A Study on a Floating Type Shrouded Wind Turbine: Design, Modeling and Analysis. *Renew. Energy* **2019**, *134*, 1099–1113. [CrossRef]
9. Singh, U.; Rizwan, M.; Malik, H.; Márquez, F.P.G. Wind Energy Scenario, Success and Initiatives towards Renewable Energy in India—A Review. *Energies* **2022**, *15*, 2291. [CrossRef]
10. Shambira, N.; Makaka, G.; Mukumba, P.; Shonhiwa, C. Comparative Analysis of Numerical Methods for Assessing Wind Potential in Fort Beaufort, South Africa, Using Two- Parameter Weibull Distribution Model. In Proceedings of the SAIP2023, the 67th Annual Conference of the South African Institute of Physics, Richards Bay, South Africa, 3–7 July 2023; Prinsloo, P.A., Ed.; South African Institute of Physics, University of Zululand: Richards Bay, South Africa, 2023; pp. 428–436.
11. Akinbami, O.M.; Oke, S.R.; Bodunrin, M.O. The State of Renewable Energy Development in South Africa: An Overview. *Alex. Eng. J.* **2021**, *60*, 5077–5093. [CrossRef]
12. Asamoah, J. Greening Electricity Generation in South Africa through Wind Energy. In Proceedings of the Greenhouse Gas Control Technologies—6th International Conference, Kyoto, Japan, 1–4 October 2002; Volume II, pp. 1349–1352.
13. Merem, E.C.; Twumasi, Y.; Wesley, J.; Olagbegi, D.; Crisler, M.; Romorno, C.; Alsarari, M.; Isokpehi, P.; Hines, A.; Hirse, G.; et al. The Evaluation of Wind Energy Potentials in South Africa. *Energy Power* **2022**, *12*, 9–25. [CrossRef]
14. Mostafaeipour, A.; Sedaghat, A.; Dehghan-Niri, A.A.; Kalantar, V. Wind Energy Feasibility Study for City of Shahrbabak in Iran. *Renew. Sustain. Energy Rev.* **2011**, *15*, 2545–2556. [CrossRef]
15. Spiru, P.; Simona, P.L. Wind Energy Resource Assessment and Wind Turbine Selection Analysis for Sustainable Energy Production. *Sci. Rep.* **2024**, *14*, 10708. [CrossRef] [PubMed]
16. McKenna, R.; Pfenninger, S.; Heinrichs, H.; Schmidt, J.; Staffell, I.; Bauer, C.; Gruber, K.; Hahmann, A.N.; Jansen, M.; Klingler, M.; et al. High-Resolution Large-Scale Onshore Wind Energy Assessments: A Review of Potential Definitions, Methodologies and Future Research Needs. *Renew. Energy* **2022**, *182*, 659–684. [CrossRef]
17. Macingwane, Z.N. Wave Energy a New Energy Mix to Produce Green Hydrogen: A Potential Future Maritime Shipping Fuel: A Study on the Port of Ngqura, Southern Africa's "Green Status Port". Master's Thesis, World Maritime University, Malmö, Sweden, 2021.
18. Mukonza, C.; Nhamo, G. Wind Energy in South Africa: A Review of Policies, Institutions and Programmes. *J. Energy S. Afr.* **2018**, *29*, 21–28. [CrossRef]
19. Gugliani, G.K.; Ley, C.; Nakhaei Rad, N.; Bekker, A. Comparison of Probability Distributions Used for Harnessing the Wind Energy Potential: A Case Study from India. *Stoch. Environ. Res. Risk Assess.* **2024**, *38*, 2213–2230. [CrossRef]
20. Tizgui, I.; El Guezar, F.; Bouzahir, H.; Benaid, B. Wind Speed Distribution Modeling for Wind Power Estimation: Case of Agadir in Morocco. *Wind Eng.* **2019**, *43*, 190–200. [CrossRef]

21. Wadi, M.; Elmasry, W. A Comparative Assessment of Five Different Distributions Based on Five Different Optimization Methods for Modeling Wind Speed Distribution. *Gazi Univ. J. Sci.* **2023**, *36*, 1096–1120. [CrossRef]
22. Okakwu, I.K.; Olabode, O.E.; Akinyele, D.O.; Ajewole, T.O. Evaluation of Wind Speed Probability Distribution Model and Sensitivity Analysis of Wind Energy Conversion System in Nigeria. *Iran. J. Electr. Electron. Eng.* **2023**, *19*, 1–15.
23. Esmaeili, L.; Naserpour, S.; Nadarajah, S. Wind Energy Potential Modeling in Northern Iran. *Stoch. Environ. Res. Risk Assess.* **2023**, *37*, 3205–3219. [CrossRef]
24. Kassem, Y.; Gökçekuş, H.; Essayah, A.M.S. Wind Power Potential Assessment at Different Locations in Lebanon: Best–Fit Probability Distribution Model and Techno-Economic Feasibility. *Eng. Technol. Appl. Sci. Res.* **2023**, *13*, 10578–10587. [CrossRef]
25. Masseran, N. Integrated Approach for the Determination of an Accurate Wind-Speed Distribution Model. *Energy Convers. Manag.* **2018**, *173*, 56–64. [CrossRef]
26. Alayat, M.M.; Kassem, Y.; Camur, H. Assessment of Wind Energy Potential as a Power Generation Source: A Case Study of Eight Selected Locations in Northern Cyprus. *Energies* **2018**, *11*, 2697. [CrossRef]
27. Wadi, M.; Elmasry, W.; Colak, I.; Jouda, M.; Kucuk, I. Utilizing Metaheuristics to Estimate Wind Energy Integration in Smart Grids with a Comparative Analysis of Ten Distributions. *Electr. Power Components Syst.* **2024**, 1–36. [CrossRef]
28. Filom, S.; Radfar, S.; Panahi, R.; Amini, E.; Neshat, M. Exploring Wind Energy Potential as a Driver of Sustainable Development in the Southern Coasts of Iran: The Importance of Wind Speed Statistical Distribution Model. *Sustainability* **2021**, *13*, 7702. [CrossRef]
29. Nymphas, E.F.; Teliat, R.O. Evaluation of the Performance of Five Distribution Functions for Estimating Weibull Parameters for Wind Energy Potential in Nigeria. *Sci. Afr.* **2024**, *23*, e02037. [CrossRef]
30. Akgül, F.G.; Şenoğlu, B. Comparison of Wind Speed Distributions: A Case Study for Aegean Coast of Turkey. *Energy Sources Part A Recover. Util. Environ. Eff.* **2023**, *45*, 2453–2470. [CrossRef]
31. Hussin, N.H.; Yusof, F. Analysis of Wind Speed Characteristics Using Probability Distribution in Johor. *Environ. Ecol. Res.* **2022**, *10*, 95–106. [CrossRef]
32. Natarajan, N.; Vasudevan, M.; Rehman, S. Evaluation of Suitability of Wind Speed Probability Distribution Models: A Case Study from Tamil Nadu, India. *Environ. Sci. Pollut. Res.* **2022**, *29*, 85855–85868. [CrossRef]
33. Atasha, N.; Norrulashikin, S.M. Fitting of Statistical Distributions to Wind Speed Data in Malaysia. *Eur. J. Sci. Res.* **2021**, *3*, 73–81.
34. Shonhiwa, C.; Makaka, G.; Mukumba, P.; Shambira, N. Investigation of Wind Power Potential in Mthatha, Eastern Cape Province, South Africa. *Appl. Sci.* **2023**, *13*, 12237. [CrossRef]
35. Khan, A.; Shafi, A. Investigation of Seasonal and Annual Wind Speed Distribution of Tarnab Based on Weibull and Rayleigh Distribution Models. *Indones. J. Earth Sci.* **2024**, *4*, A1037. [CrossRef]
36. Al-Mhairat, B.; Al-Quraan, A. Assessment of Wind Energy Resources in Jordan Using Different Optimization Techniques. *Processes* **2022**, *10*, 105. [CrossRef]
37. Komolafe, C.A.; Fadare, D.A.; Oladeji, L.B.; Gbadamosi, A.A. Evaluation of Wind Energy Potential in Omu Aran, Nigeria Using Weibull and Rayleigh Models. *Green Low-Carbon Econ.* **2023**, *2*, 131–141. [CrossRef]
38. Khan, M.A.; Zhang, Y.; Wang, J.; Wei, J.; Raza, M.A.; Ahmad, A.; Yuan, Y. Determination of Optimal Parametric Distribution and Technical Evaluation of Wind Resource Characteristics for Wind Power Potential at Jhimpir, Pakistan. *IEEE Access* **2021**, *9*, 70118–70141. [CrossRef]
39. Ali, B.; Abbas, G.; Memon, A.; Mirsaeidi, S.; Koondhar, M.A.; Chandio, S.; Channa, I.A. A Comparative Study to Analyze Wind Potential of Different Wind Corridors. *Energy Rep.* **2023**, *9*, 1157–1170. [CrossRef]
40. Saputra, H.; Sara, D.; Yanis, M. Weibull Distribution Analysis of Wind Power- Generating Potential on the Southwest Coast of Aceh, Indonesia. In *AIP Conference Proceedings*; AIP Publishing: New York, NY, USA, 2023; Volume 2613, p. 020013.
41. Younis, A.; Elshiekh, H.; Osama, D.; Shaikh-eldeen, G.; Elamir, A.; Yassin, Y.; Omer, A.; Biraima, E. Wind Speed Forecast for Sudan Using the Two-Parameter Weibull Distribution: The Case of Khartoum City. *Wind* **2023**, *3*, 213–231. [CrossRef]
42. Rehman, S.U.; Sadiq, N.; Tariq, I.; Khan, M.M.; Zahid, M.M.; Rajput, A.A.; Uddin, Z. A New Mathematical Technique and Its Python Program to Assess Wind Potential. *Beni-Suef Univ. J. Basic Appl. Sci.* **2024**, *13*, 61. [CrossRef]
43. Aries, N.; Boudia, S.M.; Ounis, H. Deep Assessment of Wind Speed Distribution Models: A Case Study of Four Sites in Algeria. *Energy Convers. Manag.* **2018**, *155*, 78–90. [CrossRef]
44. Kolesnik, S.; Rabinovitz, Y.; Byalsky, M.; Yahalom, A.; Kuperman, A. Assessment of Wind Speed Statistics in Samaria Region and Potential Energy Production. *Energies* **2023**, *16*, 3892. [CrossRef]
45. Lins, D.R.; Guedes, K.S.; Pitombeira-Neto, A.R.; Rocha, P.A.C.; de Andrade, C.F. Comparison of the Performance of Different Wind Speed Distribution Models Applied to Onshore and Offshore Wind Speed Data in the Northeast Brazil. *Energy* **2023**, *278*, 127787. [CrossRef]
46. Khan, T.; Ahmad, I.; Wang, Y.; Salam, M.; Shahzadi, A.; Batool, M. Comparison Approach for Wind Resource Assessment to Determine the Most Precise Approach. *Energy Environ.* **2022**, *35*, 1315–1338. [CrossRef]
47. Phoophiwfa, T.; Laosuwan, T.; Volodin, A.; Papukdee, N.; Suraphee, S.; Busababodhin, P. Adaptive Parameter Estimation of the Generalized Extreme Value Distribution Using Artificial Neural Network Approach. *Atmosphere* **2023**, *14*, 1197. [CrossRef]

48. Alavi, O.; Mohammadi, K.; Mostafaeipour, A. Evaluating the Suitability of Wind Speed Probability Distribution Models: A Case of Study of East and Southeast Parts of Iran. *Energy Convers. Manag.* **2016**, *119*, 101–108. [CrossRef]
49. Ahmad, Z.; Mahmoudi, E.; Alizadeh, M.; Roozegar, R.; Afify, A.Z. The Exponential T-X Family of Distributions: Properties and an Application to Insurance Data. *J. Math.* **2021**, *2021*, 3058170. [CrossRef]
50. Hellalbi, M.A.; Bouabdallah, A. Elaboration of a Generalized Mixed Model for the Wind Speed Distribution and an Assessment of Wind Energy in Algerian Coastal Regions and at the Capes. *Energy Convers. Manag.* **2024**, *305*, 118265. [CrossRef]
51. He, J.Y.; Chan, P.W.; Li, Q.S.; Huang, T.; Yim, S.H.L. Assessment of Urban Wind Energy Resource in Hong Kong Based on Multi-Instrument Observations. *Renew. Sustain. Energy Rev.* **2024**, *191*, 114123. [CrossRef]
52. Kantar, Y.M.; Usta, I.; Arik, I.; Yenilmez, I. Wind Speed Analysis Using the Extended Generalized Lindley Distribution. *Renew. Energy* **2018**, *118*, 1024–1030. [CrossRef]
53. Ali, S.; Park, H.; Noon, A.A.; Sharif, A.; Lee, D. Accuracy Testing of Different Methods for Estimating Weibull Parameters of Wind Energy at Various Heights above Sea Level. *Energies* **2024**, *17*, 2173. [CrossRef]
54. Allouhi, A.; Zamzoum, O.; Islam, M.R.; Saidur, R.; Kousksou, T.; Jamil, A.; Derouich, A. Evaluation of Wind Energy Potential in Morocco's Coastal Regions. *Renew. Sustain. Energy Rev.* **2017**, *72*, 311–324. [CrossRef]
55. Tahir, Z.U.R.; Kanwal, A.; Afzal, S.; Ali, S.; Hayat, N.; Abdullah, M.; Bin Saeed, U. Wind Energy Potential and Economic Assessment of Southeast of Pakistan. *Int. J. Green Energy* **2021**, *18*, 1–16. [CrossRef]
56. Hussain, I.; Haider, A.; Ullah, Z.; Russo, M.; Casolino, G.M.; Azeem, B. Comparative Analysis of Eight Numerical Methods Using Weibull Distribution to Estimate Wind Power Density for Coastal Areas in Pakistan. *Energies* **2023**, *16*, 1515. [CrossRef]
57. Gul, M.; Tai, N.; Huang, W.; Nadeem, M.H.; Yu, M. Evaluation of Wind Energy Potential Using an Optimum Approach Based on Maximum Distance Metric. *Sustainability* **2020**, *12*, 1999. [CrossRef]
58. El Kihel, B.; El Kadri Elyamani, N.E.; Chillali, A. Evaluation of Wind Energy Utilisation and Analysis of Turbines in the Fes Meknes Region, Kingdom of Morocco. *E3S Web Conf.* **2023**, *469*, 00025. [CrossRef]
59. Patidar, H.; Shende, V.; Baredar, P.; Soni, A. Comparative Evaluation of Optimal Weibull Parameters for Wind Power Predictions Using Numerical and Metaheuristic Optimization Methods for Different Indian Terrains. *Environ. Sci. Pollut. Res.* **2023**, *30*, 30874–30891. [CrossRef] [PubMed]
60. Amrani, F.Z.B.; Marih, S.; Missoum, I.; Boutlilis, F.; Bekkouche, B. Site Suitability Analysis of Wind Energy Resources in Different Regions of Algeria's Southwestern Highland. *Int. J. Renew. Energy Dev.* **2024**, *13*, 62–70. [CrossRef]
61. Kassem, Y.; Camur, H.; Mosbah, A.A.S. Wind Resource Evaluation in Libya: A Comparative Study of Ten Numerical Methods for the Estimation of Weibull Parameters Using Multiple Datasets. *Eng. Technol. Appl. Sci. Res.* **2024**, *14*, 13388–13397. [CrossRef]
62. Irwanto, M.; Gomesh, N.; Mamat, M.R.; Yusoff, Y.M. Assessment of Wind Power Generation Potential in Perlis, Malaysia. *Renew. Sustain. Energy Rev.* **2014**, *38*, 296–308. [CrossRef]
63. NREL. National Renewable Energy Laboratory—Wind. Available online: http://www.nrel.gov (accessed on 27 February 2025).
64. Pobočíková, I.; Michalková, M.; Sedliačková, Z.; Jurášová, D. Modelling the Wind Speed Using Exponentiated Weibull Distribution: Case Study of Poprad-Tatry, Slovakia. *Appl. Sci.* **2023**, *13*, 4031. [CrossRef]
65. Shonhiwa, C.; Makaka, G.; Mukumba, P.; Shambira, N. Determination of Optimal Geometry for an Empty Concentrator Augmented Wind Turbine. *Phys. Sci. Int. J.* **2023**, *27*, 75–90. [CrossRef]